Imaging with Noise Blending

Maarten de Hoop, Ennio Fedrizzi, Josselin Garnier, and Knut Sølna

Abstract. Seismic exploration and other imaging configurations are typically characterized by large data sets corresponding to response recordings at a set of receiver locations for the source at each of a large number of source points. Recording, storing and processing such large data sets is very resource demanding. In this paper we discuss an approach where we can reduce this work significantly without compromising imaging quality. The approach involves sounding all the sources simultaneously. We show using high-frequency asymptotics that common imaging functionals are not affected by this as long as the sources satisfy certain scaling assumptions. We refer to the approach as noise blending in the sense that the sources are blended in a particular "noisy" way so that cross-talk terms that otherwise could impede image quality with simultaneous sources are small. A significant aspect of our analysis is that we prove that the scheme is statistically stable with respect to the realization of the noise blending. We illustrate our results with numerical examples.

1. Introduction

In recent years there has been a focus on time-reversal techniques in wave propagation. A model problem that illustrates this phenomenon is the situation with a source emitting a signal that is captured on a sensor array of finite aperture, time-reversed, and re-emitted into the medium. The signal then refocuses on the original source location. The surprising result is that the focusing on the source location is often very good and in fact enhanced by randomness or heterogeneities in the medium, moreover, that the focused pulse is statistically stable and does not depend on the particular realization of the random medium. The analysis of this property involves a fourth moment calculation for the propagator. The technique has had some successful applications in the context where one can carry out physical time reversal, that is actually resend the signal physically into the medium to refocus the energy for kidney stone destruction for instance [**8**]. A challenge in the context of using the technique for imaging is that one has to migrate or resend the signal numerically in a model medium that typically does not, in general cannot, capture the heterogeneities of the original medium. The problem that we address in this paper is related in the sense that we propose to use a technique in which randomness helps the refocusing of the pulse, however, in a way that can be realized both in physical time-reversal experiments as well as in imaging contexts.

2000 *Mathematics Subject Classification.* 35R30, 35R60, 86A15, 78A46.

We consider a situation in which we actually use sources that are noisy or randomly delayed satisfying certain scaling properties. The signal is reflected off targets in the medium and recorded on a receiver array. In fact both in the case of physical time reversal as well as in the imaging context we can time reverse this signal and propagate it into the medium, either physically in (physical) time reversal or numerically in the context of imaging and obtain stable focusing at the target location. In the context of imaging the backpropagation or migration takes place in a model for the background medium. What is significant about the approach we discuss in our paper is that we sound all the sources simultaneously, both in the case of probing and backpropagation. In classic seismic exploration situations one sound one source at a time. The approach with simultaneous sources that we discuss in this paper means significant savings both in the data gathering, storing and processing stages. The analysis of the phenomenon is analogous to the analysis of the time-reversal phenomenon [**9**] and bears also similarities with techniques for passive imaging based on ambient noise sources [**1, 7, 10, 12, 15**]. The technique associated with ambient noise is another spectacular imaging situation that recently has received a lot of attention, in which one exploits the correlations in between recordings at different stations to infer some information about the medium. In this case as in the time-reversal case the presence of heterogeneities may improve the imaging result, here due to the enhanced phase space diversity that it produces.

There has been a recent focus on various blending type methods that exploits simultaneous sources, in particular in the context of seismic imaging. In the case of classic vibratory source approaches one seeks to design a family of relatively long sources encoded such that the responses of each one of them can be identified in a preprocessing step, with oil companies often having their own patented approaches for the encoding [**2, 3**]. More recently there has also been work on using simultaneous impulsive sources such as in the case of air guns that are fired with random time delays. The idea of "deblending" is to try to recover the full "single-survey" response [**3, 14**]. In fact similar techniques can also be used in the context of blending at the receiver end [**4**].

Our point of view differs somewhat from the ones above in that we are not seeking deblending approaches. We will rather present a general theoretical framework that shows how, when data are viewed through the actual image, the cross-talk effect associated with simultaneity of sources may actually be effectively mitigated by the image formation algorithm: we do not need to deblend and to estimate the full single-survey response, because the appropriate imaging algorithm will actually produce the same image as if we had the full single-survey response. We articulate explicitly the crucial scaling assumptions that should be satisfied for this to happen. Our point of view is similar to that presented in [**6**] where a least squares approach was used in the context of simultaneous sources for a particular data set and it was demonstrated how this could lead to surprisingly good results. The results obtained there are consistent with the analysis we set forth here with a probabilistic modeling of the sources.

The paper is organized as follows. In Section 2 we recall the results about the classic experimental configuration in which the full multi-static response matrix can be recorded and used. In the cases of simultaneous sources emitting either stationary random signals or randomly delayed pulses we derive and discuss the main result regarding the normal operator and its stability in Sections 3 and 4.

The applications of this result are discussed in more detail in Section 5 where we elaborate on the fascinating fact that imaging with simultaneous sources of the two types we have described gives a resolution that corresponds to the one obtained if the full multi-static response matrix was available, that is if we have the recordings of the responses at all of the receivers for all the surveys where only one source emits at a time. The main mechanism that allows us to obtain this striking result is the separation of scales that is inherent in our formulation and that serves to eliminate cross-talk terms that otherwise could contaminate an image that was constructed based on simultaneous sources. Simple numerical results are presented in Section 6.

1.1. The wave equation with random sources. We consider the solution u of the wave equation in a three-dimensional inhomogeneous medium:

$$\frac{1}{c^2(\boldsymbol{x})}\frac{\partial^2 u}{\partial t^2} - \Delta_{\boldsymbol{x}} u = n(t,\boldsymbol{x})\,. \tag{1.1}$$

The term $n(t,\boldsymbol{x})$ models the point sources emitting deterministic or random signals. For instance in the context of seismic exploration, they could be point sources emitting well separated short pulses in a sequence of experiments. We discuss this configuration in Section 2. They could be sources emitting simultaneously stationary random signals. We discuss this configuration in Section 3. They could also be simultaneous blended (i.e. time-delayed impulsive) sources emitting from the surface. We discuss this configuration in Section 4.

We write the velocity $c(\boldsymbol{x})$ in the form

$$c^{-2}(\boldsymbol{x}) = c_0^{-2}(\boldsymbol{x}) + \delta c^{-2}(\boldsymbol{x})\,,$$

where $c_0(\boldsymbol{x})$ is the known **smooth** background velocity and $\delta c^{-2}(\boldsymbol{x})$ is the velocity perturbation that we want to estimate, whose spatial support is contained in some domain $\Omega \subset \mathbb{R}^3$. The direct and inverse problems can be formulated in terms of the background Green's function that we introduce next.

1.2. The background Green's function. The solution of the wave equation (1.1) with the background velocity $c_0(\boldsymbol{x})$ has the integral representation

$$u(t,\boldsymbol{x}) = \iint G(s,\boldsymbol{x},\boldsymbol{y}) n(t-s,\boldsymbol{y}) \mathrm{d}s \mathrm{d}\boldsymbol{y}\,, \tag{1.2}$$

where $G(t,\boldsymbol{x},\boldsymbol{y})$ is the time-dependent causal Green's function. It is the fundamental solution of the wave equation

$$\frac{1}{c_0^2(\boldsymbol{x})}\frac{\partial^2 G}{\partial t^2} - \Delta_{\boldsymbol{x}} G = \delta(t)\delta(\boldsymbol{x}-\boldsymbol{y})\,, \tag{1.3}$$

starting from $G(0,\boldsymbol{x},\boldsymbol{y}) = \partial_t G(0,\boldsymbol{x},\boldsymbol{y}) = 0$, and continued on the negative time axis by $G(t,\boldsymbol{x},\boldsymbol{y}) = 0\ \forall t \le 0$.

For a homogeneous background, the Green's function in the Fourier domain is given by

$$\hat{G}(\omega,\boldsymbol{x},\boldsymbol{y}) = \frac{1}{4\pi|\boldsymbol{x}-\boldsymbol{y}|}\exp\big(i\frac{\omega}{c_0}|\boldsymbol{x}-\boldsymbol{y}|\big)\,. \tag{1.4}$$

Here the Fourier transform of a function $f(t)$ is defined by

$$\hat{f}(\omega) = \int f(t) e^{i\omega t}\mathrm{d}t\,.$$

For a general smoothly varying background, the high-frequency behavior of the Green's function is related to the travel time and it is given by the optical (or acoustical) geometric approximation [**5**]

$$\hat{G}(\omega,\boldsymbol{x},\boldsymbol{y}) \simeq \mathcal{A}(\boldsymbol{x},\boldsymbol{y}) \exp\left(i\omega\mathcal{T}(\boldsymbol{x},\boldsymbol{y})\right), \tag{1.5}$$

which is valid when the frequency ω is much larger than the inverse of the travel time $\mathcal{T}(\boldsymbol{x},\boldsymbol{y})$. Here the coefficients $\mathcal{A}(\boldsymbol{x},\boldsymbol{y})$ and $\mathcal{T}(\boldsymbol{x},\boldsymbol{y})$ are smooth except at $\boldsymbol{x}=\boldsymbol{y}$. The amplitude $\mathcal{A}(\boldsymbol{x},\boldsymbol{y})$ satisfies a transport equation and the travel time $\mathcal{T}(\boldsymbol{x},\boldsymbol{y})$ satisfies the eikonal equation.

1.3. The scattering operator. In this section we introduce the scattering operator, that is, the mapping from velocity perturbations to the data, in the Born approximation [**5**]. Our analysis pertaining to imaging and inverse scattering is based on this operator.

We assume that we observe the signals at a passive sensor array $(\boldsymbol{x}_r)_{r=1,\ldots,N_r}$ for some large time interval $[-T/2,T/2]$.

Individual sources: In the case when it is possible to emit a short pulse $f(t)$ from each point source $\boldsymbol{y}_s$, $s=1,\ldots,N_s$, then the multi-offset data are the signals $(d(t,\boldsymbol{x}_r,\boldsymbol{y}_s))_{r=1,\ldots,N_r,s=1\ldots,N_s,t\in[-T/2,T/2]}$ recorded by $\boldsymbol{x}_r$ when the source at $\boldsymbol{y}_s$ emits the short pulse at time 0. These data are modeled by the operator $\mathcal{F}_0:\ (\delta c^{-2}(\boldsymbol{x}))_{\boldsymbol{x}\in\Omega} \to (d(t,\boldsymbol{x}_r,\boldsymbol{y}_s))_{r=1,\ldots,N_r,s=1\ldots,N_s,t\in[-T/2,T/2]}$ with

$$\begin{aligned}\left(\mathcal{F}_0\delta c^{-2}\right)(t,\boldsymbol{x}_r,\boldsymbol{y}_s) &= \int_\Omega Q_0(t,\boldsymbol{x}_r,\boldsymbol{y}_s,\boldsymbol{x})\delta c^{-2}(\boldsymbol{x})\mathrm{d}\boldsymbol{x}\,,\\ Q_0(t,\boldsymbol{x}_r,\boldsymbol{y}_s,\boldsymbol{x}) &= -\frac{\partial^2}{\partial t^2}\iint G(t_2,\boldsymbol{x}_r,\boldsymbol{x})G(t_1,\boldsymbol{x},\boldsymbol{y}_s)f(t-t_1-t_2)\mathrm{d}t_1\mathrm{d}t_2\,,\end{aligned}$$

which is in the Fourier domain

$$\hat{Q}_0(\omega,\boldsymbol{x}_r,\boldsymbol{y}_s,\boldsymbol{x}) = \omega^2\hat{G}(\omega,\boldsymbol{x}_r,\boldsymbol{x})\hat{G}(\omega,\boldsymbol{x},\boldsymbol{y}_s)\hat{f}(\omega)\,. \tag{1.6}$$

Simultaneous sources: The data in the situation in which all sources emit simultaneously are the signals $(d(t,\boldsymbol{x}_r))_{r=1,\ldots,N_r,t\in[-T/2,T/2]}$ recorded by $\boldsymbol{x}_r$ with a source term $n(t,\boldsymbol{x})$ spatially supported on the set of point sources. These data are modeled by the operator $\mathcal{F}:\ (\delta c^{-2}(\boldsymbol{x}))_{\boldsymbol{x}\in\Omega} \to (d(t,\boldsymbol{x}_r))_{r=1,\ldots,N_r,t\in[-T/2,T/2]}$ with

$$\left(\mathcal{F}\delta c^{-2}\right)(t,\boldsymbol{x}_r) = \int_\Omega Q(t,\boldsymbol{x}_r,\boldsymbol{x})\delta c^{-2}(\boldsymbol{x})\mathrm{d}\boldsymbol{x}\,, \tag{1.7}$$

$$Q(t,\boldsymbol{x}_r,\boldsymbol{x}) = -\frac{\partial^2}{\partial t^2}\iiint G(t_1,\boldsymbol{x}_r,\boldsymbol{x})G(t_2,\boldsymbol{x},\boldsymbol{y})n(t-t_1-t_2,\boldsymbol{y})\mathrm{d}t_1\mathrm{d}t_2\mathrm{d}\boldsymbol{y}\,, \tag{1.8}$$

which reads in the Fourier domain as

$$\hat{Q}(\omega,\boldsymbol{x}_r,\boldsymbol{x}) = \omega^2\int \hat{G}(\omega,\boldsymbol{x}_r,\boldsymbol{x})\hat{G}(\omega,\boldsymbol{x},\boldsymbol{y})\hat{n}(\omega,\boldsymbol{y})\mathrm{d}\boldsymbol{y}\,. \tag{1.9}$$

1.4. Imaging problem. The imaging problem aims at inverting the mapping $\mathcal{F}_0$ or $\mathcal{F}$ in order to reconstruct the velocity perturbation from the data set.

When the sources can be used separately and the full data set or multi-static response matrix $\mathbf{d}=(d(t,\boldsymbol{x}_r,\boldsymbol{y}_s))_{r=1,\ldots,N_r,s=1\ldots,N_s,t\in[-T/2,T/2]}$ is available, then the usual (least-square) inversion process consists in applying the operator $(\mathcal{F}_0^*\mathcal{F}_0)^{-1}\mathcal{F}_0^*$

to the data set $\mathbf{d}$, where the adjoint of the scattering operator is

$$\big(\mathcal{F}_0^*\mathbf{d}\big)(\boldsymbol{x}) = \sum_{r=1}^{N_r}\sum_{s=1}^{N_s}\int_{-\frac{T}{2}}^{\frac{T}{2}} Q_0(t,\boldsymbol{x}_r,\boldsymbol{y}_s,\boldsymbol{x})d(t,\boldsymbol{x}_r,\boldsymbol{y}_s)\mathrm{d}t\,.$$

When simultaneous sources are used and the data set consists of the vector of recorded signals $\boldsymbol{d} = (d(t,\boldsymbol{x}_r))_{r=1,\dots,N_r,t\in[-T/2,T/2]}$ then the inversion process consists in applying the operator $(\mathcal{F}^*\mathcal{F})^{-1}\mathcal{F}^*$ to the data set $\boldsymbol{d}$, where the adjoint of the scattering operator is

$$\big(\mathcal{F}^*\boldsymbol{d}\big)(\boldsymbol{x}) = \sum_{r=1}^{N_r}\int_{-\frac{T}{2}}^{\frac{T}{2}} Q(t,\boldsymbol{x}_r,\boldsymbol{x})d(t,\boldsymbol{x}_r)\mathrm{d}t\,.$$

Note that the kernel of the adjoint $\mathcal{F}^*$ depends on the background Green's function $G(t,\boldsymbol{x},\boldsymbol{y})$ and on the source term $n(t,\boldsymbol{y})$. This means that we need to know the signals emitted by the sources in order to be able to apply the adjoint to the recorded data.

In both cases, the full least square inversion is in practice too complicated and the normal operator $\mathcal{F}_0^*\mathcal{F}_0$ or $\mathcal{F}^*\mathcal{F}$ is usually dropped in the inversion process. This procedure gives a reasonable estimate of the velocity perturbation provided the normal operator is close to the identity operator. This is approximately true for $\mathcal{F}_0^*\mathcal{F}_0$ when the multi-static response matrix is available and we will recall this result in Section 2. The purpose of this paper is to show that this is also approximately true for $\mathcal{F}^*\mathcal{F}$ in the case of two special models of random sources. In Sections 3 and 4 we will carry out a detailed statistical analysis of the kernel of the normal operator $\mathcal{F}^*\mathcal{F}$ which is given by

$$\mathcal{F}^*\mathcal{F}(\boldsymbol{x},\boldsymbol{x}') = \sum_{r=1}^{N_r}\int_{-\frac{T}{2}}^{\frac{T}{2}} Q(t,\boldsymbol{x}_r,\boldsymbol{x})Q(t,\boldsymbol{x}_r,\boldsymbol{x}')\mathrm{d}t\,. \tag{1.10}$$

We will show that the kernel is statistically stable (i.e. its fluctuations are smaller than its expectation) and that it is concentrated along the diagonal $\boldsymbol{x}\simeq\boldsymbol{x}'$.

2. Multi-offset sources

We assume in this section that multi-offset data can be recorded. The sources are localized at the points $(\boldsymbol{y}_s)_{s=1,\dots,N_s}$ and they emit short pulses $(f(t))_{t\in\mathbb{R}}$. The data acquisition is achieved during a sequence of N_s experiments. In the sth experiment, the source term in the wave equation (1.1) is

$$n(t,\boldsymbol{x}) = f(t)\delta(\boldsymbol{x}-\boldsymbol{y}_s)\,. \tag{2.1}$$

In the proof it will be important to assume that the duration of the pulse f is much smaller than the typical travel time.

The normal operator is

$$\big(\mathcal{F}_0^*\mathcal{F}_0\delta c^{-2}\big)(\boldsymbol{x}) = \int_\Omega \mathcal{F}_0^*\mathcal{F}_0(\boldsymbol{x},\boldsymbol{x}')\delta c^{-2}(\boldsymbol{x}')\mathrm{d}\boldsymbol{x}'\,, \tag{2.2}$$

with the kernel given by

$$\mathcal{F}_0^*\mathcal{F}_0(\boldsymbol{x},\boldsymbol{x}') = \sum_{r=1}^{N_r}\sum_{s=1}^{N_s}\int_{-\frac{T}{2}}^{\frac{T}{2}} Q_0(t,\boldsymbol{x}_r,\boldsymbol{y}_s,\boldsymbol{x})Q_0(t,\boldsymbol{x}_r,\boldsymbol{y}_s,\boldsymbol{x}')\mathrm{d}t\,. \tag{2.3}$$

We assume that T is large enough, so that the backscattered signals are completely recorded over $[-T/2, T/2]$. This means that T should be larger than the typical travel time for a round trip from the array to the search region. We can then replace the integral over $[-T/2, T/2]$ in (2.3) by the integral over $\mathbb{R}$. Using (1.6) and applying Parseval formula to express the quantities in the Fourier domain, we find the following expression for the kernel of the normal operator:

$$\mathcal{F}_0^*\mathcal{F}_0(\boldsymbol{x},\boldsymbol{x}') = \frac{1}{2\pi}\int \omega^4 |\hat{f}(\omega)|^2 \Big[\sum_{s=1}^{N_s} \overline{\hat{G}}\big(\omega,\boldsymbol{x},\boldsymbol{y}_s\big)\hat{G}\big(\omega,\boldsymbol{x}',\boldsymbol{y}_s\big)\Big] \times \Big[\sum_{r=1}^{N_r} \overline{\hat{G}}\big(\omega,\boldsymbol{x}_r,\boldsymbol{x}\big)\hat{G}\big(\omega,\boldsymbol{x}_r,\boldsymbol{x}'\big)\Big]\mathrm{d}\omega\,. \tag{2.4}$$

When the duration of the pulse f is much smaller than the typical travel time (which is a usual assumption), it is possible to use the high-frequency approximation of the Green's function and to perform a detailed resolution analysis which shows that the kernel $\mathcal{F}_0^*\mathcal{F}_0(\boldsymbol{x},\boldsymbol{x}')$ is concentrated along the diagonal band $\boldsymbol{x} \simeq \boldsymbol{x}'$. This comes from the fact that the two squares brackets in the expression in (2.4) behave like the kernel studied in Appendix B which is concentrated along the diagonal band. The width of the diagonal band depends on the source and receiver array apertures. If the source and receiver arrays densely sample a domain on a two-dimensional surface whose diameter is (at least) of the order of the distance from the arrays to the points $\boldsymbol{x}$ and $\boldsymbol{x}'$, then the width of the diagonal band is of the order of the wavelength.

3. Stationary random sources

In this section we consider the situation with stationary random sources. The sources are localized at the points $(\boldsymbol{y}_s)_{s=1,\ldots,N_s}$ and emit stationary random signals $(n_s(t))_{t\in\mathbb{R}}$. The source term in the wave equation (1.1) has the form

$$n(t,\boldsymbol{x}) = \sum_{s=1}^{N_s} n_s(t)\delta(\boldsymbol{x}-\boldsymbol{y}_s)\,. \tag{3.1}$$

The random functions $(n_s(t))_{t\in\mathbb{R}}$, $s = 1,\ldots,N_s$, are independent, zero-mean, stationary Gaussian processes with autocorrelation function

$$\langle n_s(t_1)n_{s'}(t_2)\rangle = \delta_{ss'}F(t_2-t_1)\,. \tag{3.2}$$

Here $\delta_{ss'}$ is the Kronecker symbol and $\langle\cdot\rangle$ stands for statistical average with respect to the distribution of the random sources. Note that we model here in terms of discrete sources at $(n_s(t))_{t\in\mathbb{R}}$, $s = 1,\ldots,N_s$. However, as we describe in Appendix A our analysis also captures the main aspects in a situation with a continuum of sources.

In the proof it is important to assume that the decoherence time of the random sources is much smaller than typical travel times, i.e. that the width of the function F is much smaller than typical travel times. The Fourier transform $\hat{F}$ of the time correlation function is a nonnegative, even real-valued function. It is proportional to the power spectral density of the sources. Note that we have

$$\big\langle \hat{n}_s(\omega)\overline{\hat{n}_{s'}(\omega')}\big\rangle = 2\pi\delta_{ss'}\hat{F}(\omega)\delta(\omega-\omega')\,. \tag{3.3}$$

Using the stationarity of the noise sources, the expectation of the kernel of the normal operator (1.10) is

$$\langle \mathcal{F}^*\mathcal{F}(\boldsymbol{x},\boldsymbol{x}')\rangle = T\sum_{r=1}^{N_r}\big\langle Q(0,\boldsymbol{x}_r,\boldsymbol{x})Q(0,\boldsymbol{x}_r,\boldsymbol{x}')\big\rangle\,.$$

Substituting the Fourier representation (1.9) into this expression and using (3.3) we find that the expectation of the kernel of the normal operator is for any T

$$\begin{aligned}\langle \mathcal{F}^*\mathcal{F}(\boldsymbol{x},\boldsymbol{x}')\rangle = \frac{T}{2\pi}\int \omega^4\hat{F}(\omega)\Big[\sum_{s=1}^{N_s}\overline{\hat{G}}\big(\omega,\boldsymbol{x},\boldsymbol{y}_s\big)\hat{G}\big(\omega,\boldsymbol{x}',\boldsymbol{y}_s\big)\Big]\\ \times\Big[\sum_{r=1}^{N_r}\overline{\hat{G}}\big(\omega,\boldsymbol{x}_r,\boldsymbol{x}\big)\hat{G}\big(\omega,\boldsymbol{x}_r,\boldsymbol{x}'\big)\Big]\mathrm{d}\omega\,.\end{aligned}\tag{3.4}$$

Note that the mean kernel has the same expression as the approximation obtained for the kernel of the normal operator (2.4) when the multi-static response matrix is available and the recording time T is larger than the typical travel time. Therefore it enjoys the same property that is is localized on the diagonal band $\boldsymbol{x}\simeq\boldsymbol{x}'$. The important question is whether the normal operator $\mathcal{F}^*\mathcal{F}$ is statistical stable, in the sense that its typical behavior is similar to the one of its expectation. From known results about the cross correlation of ambient noise signals [**10**] we anticipate that it is indeed the case when $T\to\infty$, but it is relevant to estimate carefully the fluctuations since the quantity T in typical applications cannot be taken arbitrarily large. The variance of the kernel of the normal operator is

$$\begin{aligned}\mathrm{Var}\big(\mathcal{F}^*\mathcal{F}(\boldsymbol{x},\boldsymbol{x}')\big)=\sum_{r,r'=1}^{N_r}\int_{-\frac{T}{2}}^{\frac{T}{2}}\int_{-\frac{T}{2}}^{\frac{T}{2}}\Big(\langle Q(t,\boldsymbol{x}_r,\boldsymbol{x})Q(t,\boldsymbol{x}_r,\boldsymbol{x}')Q(t',\boldsymbol{x}_{r'},\boldsymbol{x})Q(t',\boldsymbol{x}_{r'},\boldsymbol{x}')\rangle\\ -\langle Q(t,\boldsymbol{x}_r,\boldsymbol{x})Q(t,\boldsymbol{x}_r,\boldsymbol{x}')\rangle\,\langle Q(t',\boldsymbol{x}_{r'},\boldsymbol{x})Q(t',\boldsymbol{x}_{r'},\boldsymbol{x}')\rangle\Big)\mathrm{d}t\mathrm{d}t'\,.\end{aligned}\tag{3.5}$$

We can write Q in the form

$$Q(t,\boldsymbol{x}_r,\boldsymbol{x}) = \sum_{s=1}^{N_s}\int \mathcal{G}(v,\boldsymbol{x}_r,\boldsymbol{y}_s,\boldsymbol{x})n_s(t-v)\mathrm{d}v\,,\tag{3.6}$$

with

$$\mathcal{G}(v,\boldsymbol{x}_r,\boldsymbol{y}_s,\boldsymbol{x}) = -\int \partial_w^2 G(w,\boldsymbol{x}_r,\boldsymbol{x})G(v-w,\boldsymbol{x},\boldsymbol{y}_s)\mathrm{d}w\,.\tag{3.7}$$

Therefore the variance of the kernel of the normal operator can be written as

$$\mathrm{Var}\big(\mathcal{F}^*\mathcal{F}(\boldsymbol{x},\boldsymbol{x}')\big) = \sum_{r,r'=1}^{N_r}\sum_{s_1,s_2,s_1',s_2'=1}^{N_s}\iiiint \mathcal{G}(v,\boldsymbol{x}_r,\boldsymbol{y}_{s_1},\boldsymbol{x})\mathcal{G}(u,\boldsymbol{x}_r,\boldsymbol{y}_{s_2},\boldsymbol{x}')\tag{3.8}$$

$$\times\mathcal{G}(v',\boldsymbol{x}_{r'},\boldsymbol{y}_{s_1'},\boldsymbol{x})\mathcal{G}(u',\boldsymbol{x}_{r'},\boldsymbol{y}_{s_2'},\boldsymbol{x}')\mathcal{S}_{T,s_1s_2s_1's_2'}(v,u,v',u')\mathrm{d}v\mathrm{d}u\mathrm{d}v'\mathrm{d}u'\,,\tag{3.9}$$

with

$$\begin{aligned}\mathcal{S}_{T,s_1s_2s_1's_2'}(v,u,v',u') = \int_{-\frac{T}{2}}^{\frac{T}{2}}\int_{-\frac{T}{2}}^{\frac{T}{2}}\Big(\big\langle n_{s_1}(t-v)n_{s_2}(t-u)n_{s_1'}(t'-v')n_{s_2'}(t'-u')\big\rangle\\ -\big\langle n_{s_1}(t-v)n_{s_2}(t-u)\big\rangle\big\langle n_{s_1'}(t'-v')n_{s_2'}(t'-u')\big\rangle\Big)\mathrm{d}t\mathrm{d}t'\,.\end{aligned}\tag{3.10}$$

The product of second-order moments of the random processes $n_s(t)$ is

$$\big\langle n_{s_1}(t-v)n_{s_2}(t-u)\big\rangle\big\langle n_{s_1'}(t'-v')n_{s_2'}(t'-u')\big\rangle = \delta_{s_1s_2}\delta_{s_1's_2'}F(v-u)F(v'-u')\,.$$

The fourth-order moment of the Gaussian random process n is

$$\begin{aligned}\big\langle n_{s_1}(t-v)n_{s_2}(t-u)n_{s_1'}(t'-v')n_{s_2'}(t'-u')\big\rangle &= \delta_{s_1s_2}\delta_{s_1's_2'}F(v-u)F(v'-u')\\ &+\delta_{s_1s_1'}\delta_{s_2s_2'}F(t'-t-v'+v)F(t'-t-u'+u)\\ &+\delta_{s_1s_2'}\delta_{s_2s_1'}F(t'-t-u'+v)F(t'-t-v'+u)\,.\end{aligned}$$

Consequently, we have that for any $T>0$

$$\begin{aligned}&\mathcal{S}_{T,s_1s_2s_1's_2'}(v,u,v',u')\\ &\quad=\delta_{s_1s_1'}\delta_{s_2s_2'}S_T(v-v',u-u')+\delta_{s_1s_2'}\delta_{s_2s_1'}S_T(v-u',u-v')\,,\end{aligned}\tag{3.11}$$

where

$$S_T(s,u)=\frac{T^2}{4\pi^2}\iint\hat F(\omega)\hat F(\omega')\mathrm{sinc}^2\Big(\frac{(\omega-\omega')T}{2}\Big)e^{i\omega s-i\omega' u}\mathrm{d}\omega\mathrm{d}\omega'\,.\tag{3.12}$$

When T is much larger than the inverse of the bandwidth of the noise sources (i.e. T is much larger than the decoherence time), we can use the approximation

$$T\mathrm{sinc}^2\Big(\frac{(\omega-\omega')T}{2}\Big)\simeq 2\pi\delta(\omega-\omega')$$

in (3.12), and therefore

$$S_T(s,u)\simeq\frac{T}{2\pi}\int\hat F(\omega)^2e^{i\omega(s-u)}\mathrm{d}\omega\,.\tag{3.13}$$

Substituting (3.11) and (3.13) into (3.8), we obtain for all T larger than the decoherence time the following expression for the variance of the kernel $\mathcal{F}^*\mathcal{F}(\boldsymbol{x},\boldsymbol{x}')$:

$$\begin{aligned}\mathrm{Var}\big(\mathcal{F}^*\mathcal{F}(\boldsymbol{x},\boldsymbol{x}')\big)=\frac{T}{2\pi}\int\hat F(\omega)^2\omega^8\Big[\sum_{s=1}^{N_s}|\hat G\big(\omega,\boldsymbol{x},\boldsymbol{y}_s)|^2\Big]\Big[\sum_{s=1}^{N_s}|\hat G\big(\omega,\boldsymbol{x}',\boldsymbol{y}_s)|^2\Big]\\ \times\Big|\sum_{r=1}^{N_r}\overline{\hat G}\big(\omega,\boldsymbol{x}_r,\boldsymbol{x}\big)\hat G\big(\omega,\boldsymbol{x}_r,\boldsymbol{x}'\big)\Big|^2\mathrm{d}\omega\\ +\frac{T}{2\pi}\int\hat F(\omega)^2\omega^8\Big[\sum_{s=1}^{N_s}\overline{\hat G}\big(\omega,\boldsymbol{x},\boldsymbol{y}_s\big)\hat G\big(\omega,\boldsymbol{x}',\boldsymbol{y}_s\big)\Big]^2\\ \times\Big[\sum_{r=1}^{N_r}\overline{\hat G}\big(\omega,\boldsymbol{x}_r,\boldsymbol{x}\big)\hat G\big(\omega,\boldsymbol{x}_r,\boldsymbol{x}'\big)\Big]^2\mathrm{d}\omega\,.\end{aligned}\tag{3.14}$$

Using the approximation (1.5), we have in particular in the high-frequency regime for $\boldsymbol{x}=\boldsymbol{x}'$

$$\frac{\mathrm{Var}\big(\mathcal{F}^*\mathcal{F}(\boldsymbol{x},\boldsymbol{x})\big)}{\langle\mathcal{F}^*\mathcal{F}(\boldsymbol{x},\boldsymbol{x})\rangle^2}=\frac{4\pi}{T}\frac{\int\omega^8\hat F(\omega)^2\mathrm{d}\omega}{\big(\int\omega^4\hat F(\omega)\mathrm{d}\omega\big)^2}\simeq\frac{4\pi}{BT}\,,\tag{3.15}$$

where B is the bandwidth of signals emitted by the random sources. This gives the order of magnitude of the signal-to-noise ratio. Note that the ratio (3.15) does not depend on the number of source and receiver points, but only on the bandwidth B and the recording time T. Only these two parameters control the fluctuations of the kernel $\mathcal{F}^*\mathcal{F}(\boldsymbol{x},\boldsymbol{x}')$ along the diagonal band $\boldsymbol{x}\simeq\boldsymbol{x}'$.

When $\boldsymbol{x}$ is different from $\boldsymbol{x}'$ the first term in the right-hand side of (3.14) is dominant (because of the absolute values). In particular, the decay of the variance as a function of the distance $|\boldsymbol{x}-\boldsymbol{x}'|$ is ensured only by the sum over the receiver points, while the sum over the source points does not contribute to the decay, contrarily to the expectation (3.4). Therefore the relative fluctuations of the kernel $\mathcal{F}^*\mathcal{F}(\boldsymbol{x},\boldsymbol{x}')$ become larger away from the diagonal band, but we always have

$$\frac{\mathrm{Var}\big(\mathcal{F}^*\mathcal{F}(\boldsymbol{x},\boldsymbol{x}')\big)}{\langle\mathcal{F}^*\mathcal{F}(\boldsymbol{x},\boldsymbol{x})\rangle\,\langle\mathcal{F}^*\mathcal{F}(\boldsymbol{x}',\boldsymbol{x}')\rangle} \leq \frac{4\pi}{T}\frac{\int\omega^8\hat{F}(\omega)^2\mathrm{d}\omega}{\big(\int\omega^4\hat{F}(\omega)\mathrm{d}\omega\big)^2} \simeq \frac{4\pi}{BT}\,. \tag{3.16}$$

We remark that the important scaling constraint in order to ensure statistical stability is that the decoherence time of the random traces is much smaller than the recording time, that is T. Note that the total recording time, even without simultaneous sources, must be at least of the order of c_0L where L is the propagation distance. Thus, the durations of the experiments may be of the same order in the simultaneous source case as in a more classic measurement configuration with a single source at a time as long as one can generate random or heterogeneous source signals whose characteristic time scale is small compared to the travel time to the probed region. The only, but major, difference is that one performs only one experiment in the simultaneous case, while one performs N_s experiments in the classical case, where N_s is the number of sources.

4. Incoherence by blending

In this section we consider the situation in which N_s point sources emit the same short pulse waveform, but at randomly delayed times. We refer to this situation as noise blending. It is modeled by the wave equation (1.1) with a source term of the form

$$n(t,\boldsymbol{x}) = \sum_{s=1}^{N_s} f(t-\tau_s)\delta(\boldsymbol{x}-\boldsymbol{y}_s)\,. \tag{4.1}$$

The pulse function $(f(t))_{t\in\mathbb{R}}$ is deterministic. Its carrier frequency is ω_0 and its bandwidth is B. The time delays $(\tau_s)_{s=1,\dots,N_s}$ are zero-mean independent and identically distributed random variables with the probability density function $p_\tau(t)$. We denote by $\sigma_\tau^2=\langle\tau_s^2\rangle=\int t^2p_\tau(t)\mathrm{d}t$ the variance of the random time delays. Here $\langle\cdot\rangle$ stands for statistical average with respect to the distribution of the random time delays. Note that the source is not a Gaussian process, so the recorded signals are not Gaussian either, contrarily to the case addressed in the previous section, and the evaluations of second- and fourth-order moments require specific calculations which are different from the standard rules for moments of Gaussian processes.

The expectation of the kernel of the normal operator is

$$\langle\mathcal{F}^*\mathcal{F}(\boldsymbol{x},\boldsymbol{x}')\rangle = \sum_{r=1}^{N_r}\sum_{s,s'=1}^{N_s}\iint\mathcal{G}(u,\boldsymbol{x}_r,\boldsymbol{y}_s,\boldsymbol{x})\mathcal{G}(u',\boldsymbol{x}_r,\boldsymbol{y}_{s'},\boldsymbol{x}')\mathcal{I}_{T,ss'}(u,u')\mathrm{d}u\mathrm{d}u'\,, \tag{4.2}$$

where $\mathcal{G}$ is given by (3.7) and $\mathcal{I}_{T,ss'}$ is defined by

$$\mathcal{I}_{T,ss'}(u,u') = \int_{-\frac{T}{2}}^{\frac{T}{2}}\big\langle f(t-u-\tau_s)f(t-u'-\tau_{s'})\big\rangle\mathrm{d}t\,. \tag{4.3}$$

We assume that T is large enough, so that the backscattered signals are completely recorded over $[-T/2, T/2]$. This means that T should be larger than the typical travel time from the array to the search region and than the typical time delay σ_τ. We can then replace the integral over $[-T/2, T/2]$ in (4.3) by the integral over $\mathbb{R}$ and we find

$$\mathcal{I}_{T,ss'}(u,u') = \frac{1}{2\pi}\int |\hat{f}(\omega)|^2 e^{-i\omega(u-u')}\big\langle e^{-i\omega(\tau_s-\tau_{s'})}\big\rangle \mathrm{d}\omega\,.$$

If $s \neq s'$, then

$$\big\langle e^{-i\omega(\tau_s-\tau_{s'})}\big\rangle = \big|\big\langle e^{i\omega\tau_s}\big\rangle\big|^2 = |\hat{p}_\tau(\omega)|^2\,.$$

Therefore, if $\sigma_\tau\omega_0 \gg 1$ then $|\hat{p}_\tau(\omega)|^2 \simeq 0$ for all ω in the bandwidth and

$$\mathcal{I}_{T,ss'}(u,u') = \begin{cases} \frac{1}{2\pi}\int |\hat{f}(\omega)|^2 e^{-i\omega(u-u')}\mathrm{d}\omega & \text{if } s = s', \\ 0 & \text{otherwise.} \end{cases}$$

This result shows that the expectation of the kernel of the normal operator is

$$\begin{aligned}\langle \mathcal{F}^*\mathcal{F}(\boldsymbol{x},\boldsymbol{x}')\rangle = \frac{1}{2\pi}\int \omega^4 |\hat{f}(\omega)|^2 \Big[\sum_{s=1}^{N_s} \overline{\hat{G}}\big(\omega,\boldsymbol{x},\boldsymbol{y}_s\big)\hat{G}\big(\omega,\boldsymbol{x}',\boldsymbol{y}_s\big)\Big] \\ \times\Big[\sum_{r=1}^{N_r} \overline{\hat{G}}\big(\omega,\boldsymbol{x}_r,\boldsymbol{x}\big)\hat{G}\big(\omega,\boldsymbol{x}_r,\boldsymbol{x}'\big)\Big]\mathrm{d}\omega\,,\end{aligned} \tag{4.4}$$

which has the same form and the same properties (in terms of concentration along the diagonal $\boldsymbol{x} \simeq \boldsymbol{x}'$) as the expectation of the kernel of the normal operator (3.4) in the case of stationary random sources, or as the kernel of the normal operator (2.4) obtained when the full multi-static response matrix is available. The important issue to be clarified is the statistical stability of the normal operator $\mathcal{F}^*\mathcal{F}$.

The analysis of the variance of the kernel of the normal operator is based on the following basic result: for any $u, u', \tilde{u}, \tilde{u}' \in \mathbb{R}$ and $s, s', \tilde{s}, \tilde{s}' = 1, \ldots, N_s$, and again for T much larger than the typical travel time and time delay,

$$\begin{aligned}\mathcal{J} :=& \int_{-\frac{T}{2}}^{\frac{T}{2}}\int_{-\frac{T}{2}}^{\frac{T}{2}}\Big(\big\langle f(t-u-\tau_s)f(t-u'-\tau_{s'})f(\tilde{t}-\tilde{u}-\tau_{\tilde{s}})f(\tilde{t}-\tilde{u}'-\tau_{\tilde{s}'})\big\rangle \\ &-\big\langle f(t-u-\tau_s)f(t-u'-\tau_{s'})\big\rangle\big\langle f(\tilde{t}-\tilde{u}-\tau_{\tilde{s}})f(\tilde{t}-\tilde{u}'-\tau_{\tilde{s}'})\big\rangle\Big)\mathrm{d}t\mathrm{d}\tilde{t} \\ \simeq& \frac{1}{(2\pi)^2}\iint |\hat{f}(\omega)|^2|\hat{f}(\tilde{\omega})|^2 e^{-i\omega(u-u')}e^{-i\tilde{\omega}(\tilde{u}-\tilde{u}')} \\ &\times\big[\big\langle e^{-i\omega(\tau_s-\tau_{s'})}e^{-i\tilde{\omega}(\tau_{\tilde{s}}-\tau_{\tilde{s}'})}\big\rangle - \big\langle e^{-i\omega(\tau_s-\tau_{s'})}\big\rangle\big\langle e^{-i\tilde{\omega}(\tau_{\tilde{s}}-\tau_{\tilde{s}'})}\big\rangle\big]\mathrm{d}\omega\mathrm{d}\tilde{\omega}\,.\end{aligned}$$

If $\sigma_\tau\omega_0 \gg 1$, then

$$\begin{aligned}\mathcal{J} =& \delta_{s\tilde{s}}\delta_{s'\tilde{s}'}(1-\delta_{ss'})\frac{1}{(2\pi)^2}\iint |\hat{f}(\omega)|^2|\hat{f}(\tilde{\omega})|^2 e^{-i\omega(u-u')}e^{-i\tilde{\omega}(\tilde{u}-\tilde{u}')}|\hat{p}_\tau(\omega+\tilde{\omega})|^2\mathrm{d}\omega\mathrm{d}\tilde{\omega} \\ &+\delta_{s\tilde{s}'}\delta_{s'\tilde{s}}(1-\delta_{ss'})\frac{1}{(2\pi)^2}\iint |\hat{f}(\omega)|^2|\hat{f}(\tilde{\omega})|^2 e^{-i\omega(u-u')}e^{-i\tilde{\omega}(\tilde{u}-\tilde{u}')}|\hat{p}_\tau(\omega-\tilde{\omega})|^2\mathrm{d}\omega\mathrm{d}\tilde{\omega}\,.\end{aligned}$$

Therefore the variance of the kernel $\mathcal{F}^*\mathcal{F}(\boldsymbol{x},\boldsymbol{x}')$ is:

$$\begin{aligned}
\mathrm{Var}\big(\mathcal{F}^*\mathcal{F}(\boldsymbol{x},\boldsymbol{x}')\big) &= \frac{1}{(2\pi)^2}\iint \mathrm{d}\omega\mathrm{d}\tilde\omega|\hat f(\omega)|^2\omega^4|\hat f(\tilde\omega)|^2\tilde\omega^4\\
&\times\Big[\sum_{r=1}^{N_r}\overline{\hat G}\big(\omega,\boldsymbol{x}_r,\boldsymbol{x}\big)\hat G\big(\omega,\boldsymbol{x}_r,\boldsymbol{x}'\big)\Big]\Big[\sum_{r=1}^{N_r}\overline{\hat G}\big(\tilde\omega,\boldsymbol{x}_r,\boldsymbol{x}\big)\hat G\big(\tilde\omega,\boldsymbol{x}_r,\boldsymbol{x}'\big)\Big]\\
&\times\Big[\sum_{s,s'=1,s\neq s'}^{N_s}\overline{\hat G}\big(\omega,\boldsymbol{x},\boldsymbol{y}_s\big)\overline{\hat G}\big(\tilde\omega,\boldsymbol{x},\boldsymbol{y}_s\big)\hat G\big(\omega,\boldsymbol{x}',\boldsymbol{y}_{s'}\big)\hat G\big(\tilde\omega,\boldsymbol{x}',\boldsymbol{y}_{s'}\big)|\hat p_\tau(\omega+\tilde\omega)|^2\\
&\quad+\sum_{s,s'=1,s\neq s'}^{N_s}\overline{\hat G}\big(\omega,\boldsymbol{x},\boldsymbol{y}_s\big)\hat G\big(\tilde\omega,\boldsymbol{x}',\boldsymbol{y}_s\big)\overline{\hat G}\big(\tilde\omega,\boldsymbol{x},\boldsymbol{y}_{s'}\big)\hat G\big(\omega,\boldsymbol{x}',\boldsymbol{y}_{s'}\big)|\hat p_\tau(\omega-\tilde\omega)|^2\Big],
\end{aligned}$$

that we can also write as (after the change of variable $\tilde\omega\to-\tilde\omega$ in the first part of the right member)

$$\begin{aligned}
\mathrm{Var}\big(\mathcal{F}^*\mathcal{F}(\boldsymbol{x},\boldsymbol{x}')\big) &= \frac{1}{(2\pi)^2}\iint \mathrm{d}\omega\mathrm{d}\tilde\omega|\hat f(\omega)|^2\omega^4|\hat f(\tilde\omega)|^2\tilde\omega^4\\
&\times\Big[\sum_{r=1}^{N_r}\overline{\hat G}\big(\omega,\boldsymbol{x}_r,\boldsymbol{x}\big)\hat G\big(\omega,\boldsymbol{x}_r,\boldsymbol{x}'\big)\Big]\Big[\sum_{r=1}^{N_r}\hat G\big(\tilde\omega,\boldsymbol{x}_r,\boldsymbol{x}\big)\overline{\hat G}\big(\tilde\omega,\boldsymbol{x}_r,\boldsymbol{x}'\big)\Big]\\
&\times\Big\{\Big[\sum_{s=1}^{N_s}\overline{\hat G}\big(\omega,\boldsymbol{x},\boldsymbol{y}_s\big)\hat G\big(\tilde\omega,\boldsymbol{x},\boldsymbol{y}_s\big)\Big]\Big[\sum_{s=1}^{N_s}\hat G\big(\omega,\boldsymbol{x}',\boldsymbol{y}_s\big)\overline{\hat G}\big(\tilde\omega,\boldsymbol{x}',\boldsymbol{y}_s\big)\Big]\\
&\quad-\sum_{s=1}^{N_s}\overline{\hat G}\big(\omega,\boldsymbol{x},\boldsymbol{y}_s\big)\hat G\big(\tilde\omega,\boldsymbol{x},\boldsymbol{y}_s\big)\hat G\big(\omega,\boldsymbol{x}',\boldsymbol{y}_s\big)\overline{\hat G}\big(\tilde\omega,\boldsymbol{x}',\boldsymbol{y}_s\big)\Big\}|\hat p_\tau(\omega-\tilde\omega)|^2\\
&\quad+\frac{1}{(2\pi)^2}\iint \mathrm{d}\omega\mathrm{d}\tilde\omega|\hat f(\omega)|^2\omega^4|\hat f(\tilde\omega)|^2\tilde\omega^4\\
&\times\Big[\sum_{r=1}^{N_r}\overline{\hat G}\big(\omega,\boldsymbol{x}_r,\boldsymbol{x}\big)\hat G\big(\omega,\boldsymbol{x}_r,\boldsymbol{x}'\big)\Big]\Big[\sum_{r=1}^{N_r}\overline{\hat G}\big(\tilde\omega,\boldsymbol{x}_r,\boldsymbol{x}\big)\hat G\big(\tilde\omega,\boldsymbol{x}_r,\boldsymbol{x}'\big)\Big]\\
&\times\Big\{\Big[\sum_{s=1}^{N_s}\overline{\hat G}\big(\omega,\boldsymbol{x},\boldsymbol{y}_s\big)\hat G\big(\tilde\omega,\boldsymbol{x}',\boldsymbol{y}_s\big)\Big]\Big[\sum_{s=1}^{N_s}\overline{\hat G}\big(\tilde\omega,\boldsymbol{x},\boldsymbol{y}_s\big)\hat G\big(\omega,\boldsymbol{x}',\boldsymbol{y}_s\big)\Big]\\
&\quad-\sum_{s=1}^{N_s}\overline{\hat G}\big(\omega,\boldsymbol{x},\boldsymbol{y}_s\big)\hat G\big(\tilde\omega,\boldsymbol{x}',\boldsymbol{y}_s\big)\overline{\hat G}\big(\tilde\omega,\boldsymbol{x},\boldsymbol{y}_s\big)\hat G\big(\omega,\boldsymbol{x}',\boldsymbol{y}_s\big)\Big\}|\hat p_\tau(\omega-\tilde\omega)|^2\,.
\end{aligned}\tag{4.5}$$

The statistical stability follows from the fact that the variance of the kernel is small. In order to prove that the variance is small we first want to show that the integral in $(\omega,\tilde\omega)$ concentrates on a small band around the diagonal $\omega=\tilde\omega$. The double integral in $(\omega,\tilde\omega)$ can be written as a double integral in $(\frac{\omega+\tilde\omega}{2},\omega-\tilde\omega)$. The products of terms that depend on $\hat G$ vary in $\omega-\tilde\omega$ on a scale of the order of the reciprocal of the typical travel time c_0/L (where L is the typical propagation distance). This can be seen from the high-frequency asymptotic expression (1.5) of the Green's function. Moreover, the terms depending on $\hat f$ are varying in $\omega-\tilde\omega$ on a scale of the order B and that the term $|\hat p_\tau(\omega-\tilde\omega)|^2$ concentrates on a band of size $|\omega-\tilde\omega|<\sigma_\tau^{-1}$.

Therefore, provided $\sigma_\tau^{-1} \ll \min(c_0/L, B)$, we can make the approximation

$$|\hat{p}_\tau(\omega-\tilde{\omega})|^2 \simeq \frac{2\pi}{T_\tau}\delta(\omega-\tilde{\omega})\,, \quad \text{with} \quad \frac{1}{T_\tau} = \int p_\tau^2(t)\mathrm{d}t\,.$$

To summarize, if $\sigma_\tau \gg L/c_0$ and $\sigma_\tau B \gg 1$, then the variance of the kernel $\mathcal{F}^*\mathcal{F}(\boldsymbol{x},\boldsymbol{x}')$ is:

$$\begin{aligned}
\mathrm{Var}\big(\mathcal{F}^*\mathcal{F}(\boldsymbol{x},\boldsymbol{x}')\big) &= \frac{1}{2\pi T_\tau}\int \mathrm{d}\omega |\hat{f}(\omega)|^4\omega^8 \Big|\sum_{r=1}^{N_r}\overline{\hat{G}}\big(\omega,\boldsymbol{x}_r,\boldsymbol{x}\big)\hat{G}\big(\omega,\boldsymbol{x}_r,\boldsymbol{x}'\big)\Big|^2 \\
&\times\Big\{\Big[\sum_{s=1}^{N_s}|\hat{G}\big(\omega,\boldsymbol{x},\boldsymbol{y}_s\big)|^2\Big]\Big[\sum_{s=1}^{N_s}|\hat{G}\big(\omega,\boldsymbol{x}',\boldsymbol{y}_s\big)|^2\Big] - \sum_{s=1}^{N_s}|\hat{G}\big(\omega,\boldsymbol{x},\boldsymbol{y}_s\big)|^2|\hat{G}\big(\omega,\boldsymbol{x}',\boldsymbol{y}_s\big)|^2\Big\} \\
&\quad + \frac{1}{2\pi T_\tau}\int \mathrm{d}\omega |\hat{f}(\omega)|^4\omega^8\Big[\sum_{r=1}^{N_r}\overline{\hat{G}}\big(\omega,\boldsymbol{x}_r,\boldsymbol{x}\big)\hat{G}\big(\omega,\boldsymbol{x}_r,\boldsymbol{x}'\big)\Big]^2 \\
&\times\Big\{\Big[\sum_{s=1}^{N_s}\overline{\hat{G}}\big(\omega,\boldsymbol{x},\boldsymbol{y}_s\big)\hat{G}\big(\omega,\boldsymbol{x}',\boldsymbol{y}_s\big)\Big]^2 - \sum_{s=1}^{N_s}\overline{\hat{G}}\big(\omega,\boldsymbol{x},\boldsymbol{y}_s\big)^2\hat{G}\big(\omega,\boldsymbol{x}',\boldsymbol{y}_s\big)^2\Big\}\,.
\end{aligned}$$

The hypothesis $\sigma_\tau B \gg 1$ is not restrictive and it was already required in the framework of the stationary random sources in section 3. The hypothesis $\sigma_\tau \gg L/c_0$ means that the random time delays, and therefore the recording time, must be larger than the typical travel time. We will see in the numerical illustrations that it is enough to have random time shifts of the same order of typical travel time.

We have in particular for $\boldsymbol{x} = \boldsymbol{x}'$

$$\frac{\mathrm{Var}\big(\mathcal{F}^*\mathcal{F}(\boldsymbol{x},\boldsymbol{x})\big)}{\langle\mathcal{F}^*\mathcal{F}(\boldsymbol{x},\boldsymbol{x})\rangle^2} \simeq \frac{4\pi}{T_\tau}\big(1-\frac{1}{N_s}\big)\frac{\int\omega^8|\hat{f}(\omega)|^4\mathrm{d}\omega}{\big(\int\omega^4|\hat{f}(\omega)|^2\mathrm{d}\omega\big)^2} \simeq \frac{4\pi}{BT_\tau}\,. \tag{4.6}$$

This gives the order of magnitude of the signal-to-noise ratio. The quantity BT_τ controls the statistical stability. It should be large so that the kernel $\mathcal{F}^*\mathcal{F}(\boldsymbol{x},\boldsymbol{x}')$ is statistically stable. Using the method of Lagrange multipliers we get the two following results:

The maximal value of T_τ amongst all probability density functions p_τ compactly supported in $[-\tau_{\max},\tau_{\max}]$ is $T_\tau = 2\tau_{\max}$ and it is obtained for a uniform density over $[-\tau_{\max},\tau_{\max}]$.

The maximal value of T_τ amongst all probability density functions p_τ with variance σ_τ^2 is $T_\tau = \frac{5\sqrt{5}}{3}\sigma_\tau$ and it is obtained for a probability density function of the form

$$p_\tau(t) = \frac{3}{4\sqrt{5}\sigma_\tau}\big(1-\frac{t^2}{5\sigma_\tau^2}\big)\mathbf{1}_{[-\sqrt{5}\sigma_\tau,\sqrt{5}\sigma_\tau]}(t)\,.$$

5. Applications

5.1. Simultaneous source exploration. In this section we consider the formulation (1.1)-(4.1) as it describes a physical exploration problem. That is, the source term $n(t,\boldsymbol{x})$ results from the simultaneous emission of N_s point sources located at $(\boldsymbol{y}_s)_{s=1,\dots,N_s}$ and emitting randomly delayed pulses as in (4.1), and from the measurements at the N_r receiver points $(\boldsymbol{x}_r)_{r=1,\dots,N_r}$ we aim to recover the medium perturbations $(\delta c^{-2}(\boldsymbol{x}))_{\boldsymbol{x}\in\Omega}$. In this framework, only one experiment is performed to acquire the data set.

To put our approach in perspective we first consider the classic experimental configuration in which we can use the sources separately and we observe the full multi-static response matrix $\mathbf{d} = (d(t, \boldsymbol{x}_r, \boldsymbol{y}_s))_{r=1,\dots,N_r, s=1\dots,N_s, t\in[-T/2,T/2]}$. This requires us to perform N_s experiments. In the sth experiment, $s = 1, \dots, N_s$, we observe the signal $d(t, \boldsymbol{x}_r, \boldsymbol{y}_s)$ at the receiver point $\boldsymbol{x}_r$ when the point source at $\boldsymbol{y}_s$ emits a short pulse $f(t)$. The Reverse-Time imaging functional for the estimation of the medium perturbations δc^{-2} is based on the application of the adjoint $\mathcal{F}_0^*$ on the data set [**5**]:

$$\begin{aligned}\mathcal{I}_{\rm RT}(\boldsymbol{x}) = \big(\mathcal{F}_0^*\mathbf{d}\big)(\boldsymbol{x}) &= \sum_{s=1}^{N_s}\sum_{r=1}^{N_r}\int Q_0(t,\boldsymbol{x}_r,\boldsymbol{y}_s,\boldsymbol{x})d(t,\boldsymbol{x}_r,\boldsymbol{y}_s)\mathrm{d}t \\ &= \frac{1}{2\pi}\sum_{s=1}^{N_s}\sum_{r=1}^{N_r}\int \omega^2\hat{G}(\omega,\boldsymbol{x},\boldsymbol{x}_r)\hat{G}(\omega,\boldsymbol{x},\boldsymbol{y}_s)\hat{f}(\omega)\overline{\hat{d}}(\omega,\boldsymbol{x}_r,\boldsymbol{y}_s)\mathrm{d}\omega\,. \qquad (5.1)\end{aligned}$$

To evaluate the imaging functional, one needs a priori to solve $N_s + N_r$ times the wave equation in order to get $\hat{G}(\omega, \boldsymbol{x}, \boldsymbol{x}_r)$, for $r = 1, \dots, N_r$, and $\hat{G}(\omega, \boldsymbol{x}, \boldsymbol{y}_s)$, for $s = 1, \dots, N_s$. Usually the number of sources is smaller than the number of receivers $N_s < N_r$ and then the strategy that requires to call the numerical wave solver only $2N_s$ times is as follows:
- for each $s = 1, \dots, N_s$, compute the wave emitted by the source at $\boldsymbol{y}_s$, that is to say evaluate $\hat{v}^{(s)}(\omega, \boldsymbol{x})$ solution of the Helmholtz equation with the background velocity $c_0(\boldsymbol{x})$ and with the source term $\hat{n}(\omega, \boldsymbol{x}) = \omega^2\hat{f}(\omega)\delta(\boldsymbol{x} - \boldsymbol{y}_s)$.
- for each $s = 1, \dots, N_s$, time reverse the recorded data and propagate these time reversed signals from the receivers, that is to say evaluate $\hat{u}^{(s)}(\omega, \boldsymbol{x})$ solution of the Helmholtz equation with the background velocity $c_0(\boldsymbol{x})$ and with the source term $\hat{n}(\omega, \boldsymbol{x}) = \sum_{r=1}^{N_r}\overline{\hat{d}}(\omega, \boldsymbol{x}_r, \boldsymbol{y}_s)\delta(\boldsymbol{x} - \boldsymbol{x}_r)$.
- for each $s = 1, \dots, N_s$, correlate the two pairs of signals, one of them being time-reversed first, and sum over the sources. One gets

$$\mathcal{I}_{\rm RT}(\boldsymbol{x}) = \frac{1}{2\pi}\sum_{s=1}^{N_s}\int \hat{v}^{(s)}(\omega,\boldsymbol{x})\hat{u}^{(s)}(\omega,\boldsymbol{x})\mathrm{d}\omega\,,$$

which is equal to (5.1). In the Born approximation and for T large enough (i.e. larger than the typical travel time), then we get

$$\begin{aligned}\mathcal{I}_{\rm RT}(\boldsymbol{x}) &\approx \int_\Omega \mathcal{K}(\boldsymbol{x},\boldsymbol{x}')\delta c^{-2}(\boldsymbol{x}')\mathrm{d}\boldsymbol{x}'\,, \\ \mathcal{K}(\boldsymbol{x},\boldsymbol{x}') = \big(\mathcal{F}_0^*\mathcal{F}_0\big)(\boldsymbol{x},\boldsymbol{x}') &= \frac{1}{2\pi}\int \omega^4|\hat{f}(\omega)|^2\Big[\sum_{s=1}^{N_s}\overline{\hat{G}}\big(\omega,\boldsymbol{x},\boldsymbol{y}_s\big)\hat{G}\big(\omega,\boldsymbol{x}',\boldsymbol{y}_s\big)\Big] \\ &\quad\times\Big[\sum_{r=1}^{N_r}\overline{\hat{G}}\big(\omega,\boldsymbol{x}_r,\boldsymbol{x}\big)\hat{G}\big(\omega,\boldsymbol{x}_r,\boldsymbol{x}'\big)\Big]\mathrm{d}\omega\,. \qquad (5.2)\end{aligned}$$

It is possible to equalize the spectrum and to divide the data by $\omega^4|\hat{f}(\omega)|^2$ in the Fourier domain over the bandwidth in order to improve the accuracy of the estimation. We will see below that this functional gives an image of the velocity perturbations δc^{-2} with an accuracy of the order of the wavelength when the source and receiver array apertures are large enough.

We then return to the blended source configuration (1.1)-(4.1). In this case the data set consists of the vector $\boldsymbol{d} = (d(t, \boldsymbol{x}_r))_{r=1,\dots,N_r, t\in[-T/2,T/2]}$, where $d(t, \boldsymbol{x}_r)$ is the signal measured at $\boldsymbol{x}_r$ when the source term is (4.1). The imaging functional (for imaging the medium perturbations) consists in applying the adjoint operator $\mathcal{F}^*$ to the data set:

$$\mathcal{I}_{\rm BS}(\boldsymbol{x}) = \big(\mathcal{F}^*\boldsymbol{d}\big)(\boldsymbol{x}) = \sum_{r=1}^{N_r} \int Q(t, \boldsymbol{x}_r, \boldsymbol{x}) d(t, \boldsymbol{x}_r) {\rm d}t$$

$$= \frac{1}{2\pi} \sum_{r=1}^{N_r} \sum_{s=1}^{N_s} \iint \omega^2 \hat{G}(\omega, \boldsymbol{x}, \boldsymbol{x}_r) \hat{G}(\omega, \boldsymbol{x}, \boldsymbol{y}) \hat{n}(\omega, \boldsymbol{y}) \overline{\hat{d}}(\omega, \boldsymbol{x}_r) {\rm d}\boldsymbol{y} {\rm d}\omega \,. \tag{5.3}$$

To evaluate the imaging functional, one needs to solve the wave equation only two times. This is a considerable advantage compared to the standard technique described above that uses the full response matrix and that requires $2N_s$ calls to the numerical wave solver. More precisely the strategy to evaluate the imaging functional is as follows:

- compute the wave emitted by the original source $n(t, \boldsymbol{x})$ given by (4.1), that is to say evaluate $\hat{v}(\omega, \boldsymbol{x})$ solution of the Helmholtz equation with the background velocity $c_0(\boldsymbol{x})$ and with the source term $\hat{n}(\omega, \boldsymbol{x})\omega^2$.
- time reverse the recorded data and propagate these time reversed signals from the receivers, that is to say evaluate $\hat{u}(\omega, \boldsymbol{x})$ solution of the Helmholtz equation with the background velocity $c_0(\boldsymbol{x})$ and with the source term $\hat{n}(\omega, \boldsymbol{x}) = \sum_{r=1}^{N_r} \overline{\hat{d}}(\omega, \boldsymbol{x}_r)\delta(\boldsymbol{x} - \boldsymbol{x}_r)$.
- correlate the two pairs of signals, one of them being time-reversed first. One gets

$$\mathcal{I}_{\rm BS}(\boldsymbol{x}) = \frac{1}{2\pi} \int \hat{v}(\omega, \boldsymbol{x}) \hat{u}(\omega, \boldsymbol{x}) {\rm d}\omega \,,$$

which is equal to (5.3). In the Born approximation and for T large enough (i.e. larger than the typical travel time and the typical time delay), then we then find that

$$\mathcal{I}_{\rm BS}(\boldsymbol{x}) = \int_\Omega \mathcal{F}^*\mathcal{F}(\boldsymbol{x}, \boldsymbol{x}') \delta c^{-2}(\boldsymbol{x}') {\rm d}\boldsymbol{x}' \approx \int_\Omega \langle \mathcal{F}^*\mathcal{F}(\boldsymbol{x}, \boldsymbol{x}') \rangle \, \delta c^{-2}(\boldsymbol{x}') {\rm d}\boldsymbol{x}'$$

$$= \int_\Omega \mathcal{K}(\boldsymbol{x}, \boldsymbol{x}') \delta c^{-2}(\boldsymbol{x}') {\rm d}\boldsymbol{x}' \,, \tag{5.4}$$

where the kernel $\mathcal{K}(\boldsymbol{x}, \boldsymbol{x}')$ is given by (5.2). Note that here we have used the crucial stabilization result $\mathcal{F}^*\mathcal{F} \simeq \langle \mathcal{F}^*\mathcal{F} \rangle$ that we derived in Section 4.

The resolution in the perturbation estimate is given by the classic Kirchhoff resolution which characterizes the support of $\mathcal{K}$ [**11**]. We assume that the source and receiver arrays coincide and have a characteristic aperture or diameter a. Then:

(i) If the diameter a of the array is smaller than the distance L from the array to the target, the resolution is given by the standard Rayleigh resolution formulas: The cross range resolution is $\lambda_0 L/a$ and the range resolution is $\lambda_0 (L/a)^2$ for narrowband sources and c_0/B for broadband sources with bandwidth $B > \omega_0 (a/L)^2$. Here λ_0 is the central wavelength corresponding to the central frequency ω_0 of the pulse wave form f.

(ii) If the diameter of the array is of the same order as or larger than the distance from the array to the target, then we find that the resolution is of the order of the central wavelength λ_0.

Note that we could also use the stationary random sources of the form (3.1) that in view of (4.4) gives the same resolution as the noise blended sources. Our analysis applies directly to the important case when we do not have "controlled sources", rather "sources of opportunity". However the important assumption that we make here is that the (incoherent) traces of the sources and their locations are assumed to be known. Situations in which the sources are not assumed a priori known are discussed in [**13**].

5.2. Seismic forward simulations. We illustrate here how our results could be used in the context of forward simulations which constitute an important ingredient in typical iterative imaging or inversion schemes.

Consider again first the situation when we in fact have measured the full multi-static response (MSR) matrix $\mathbf{d} = (d(t, \boldsymbol{x}_r, \boldsymbol{y}_s))_{r=1,\ldots,N_r, s=1,\ldots,N_s, t\in[-T/2,T/2]}$. For each $s = 1, \ldots, N_s$, denote by $u^{(s)}(t, \boldsymbol{x}; \hat{c})$ the numerical solution of (1.1) with the source term $n(t, \boldsymbol{x}) = \delta(\boldsymbol{x} - \boldsymbol{y}_s)f(t)$ when the medium perturbations are $\delta\hat{c}^{-2}$. Denote by $\mathbf{d}[\hat{c}]$ the corresponding computed MSR matrix, whose elements are defined by

$$d[\hat{c}](t, \boldsymbol{x}_r, \boldsymbol{y}_s) = u^{(s)}(t, \boldsymbol{x}_r; \hat{c}) = \big(\mathcal{F}_0\delta\hat{c}^{-2}\big)(t, \boldsymbol{x}_r, \boldsymbol{y}_s)\,.$$

An iterative imaging scheme can then be based on calculating and minimizing the quadratic misfit functional

$$\mathcal{J}[\hat{c}] = \sum_{s=1}^{N_s}\sum_{r=1}^{N_r}\int_{-\frac{T}{2}}^{\frac{T}{2}} \big|d(t, \boldsymbol{x}_r, \boldsymbol{y}_s) - d[\hat{c}](t, \boldsymbol{x}_r, \boldsymbol{y}_s)\big|^2\mathrm{d}t\,. \tag{5.5}$$

The implementation of a descent algorithm over $\hat{c}$ produces a sequence of estimates $\hat{c}_1, \hat{c}_2, \ldots$ leading to an estimate, say $\hat{c}_N$, of c at termination. We find in the Born approximation that the residual in (5.5) is

$$\begin{aligned}\mathcal{J}[\hat{c}] &= \sum_{s=1}^{N_s}\sum_{r=1}^{N_r}\int_{-\frac{T}{2}}^{\frac{T}{2}} \big|\big(\mathcal{F}_0\delta c^{-2}\big)(t, \boldsymbol{x}_r, \boldsymbol{y}_s) - \big(\mathcal{F}_0\delta\hat{c}^{-2}\big)(t, \boldsymbol{x}_r, \boldsymbol{y}_s)\big|^2\mathrm{d}t\\ &= \iint_{\Omega^2} \mathcal{F}_0^*\mathcal{F}_0(\boldsymbol{x}, \boldsymbol{x}')(\delta c^{-2}(\boldsymbol{x}) - \delta\hat{c}^{-2}(\boldsymbol{x}))(\delta c^{-2}(\boldsymbol{x}') - \delta\hat{c}^{-2}(\boldsymbol{x}'))\mathrm{d}\boldsymbol{x}\mathrm{d}\boldsymbol{x}'\,,\end{aligned} \tag{5.6}$$

with $\mathcal{F}_0^*\mathcal{F}_0(\boldsymbol{x}, \boldsymbol{x}')$ defined by (2.4) when T is large enough (i.e. larger than the typical travel time). Note that this minimization approach requires the calculation of $\mathcal{J}[\hat{c}_j]$, $j = 1, \ldots, N$ which is computationally very expensive because it requires computing the full multi-static response matrix with a new velocity function at each step, which amounts to solving the forward problem N_s times at each step.

Consider now the situation when the sources are defined as in (4.1), that is with simultaneous randomly delayed point sources. The data has the form of the vector $\boldsymbol{d} = (d(t, \boldsymbol{x}_r))_{r=1,\ldots,N_r, t\in[-T/2,T/2]}$. Denote by $u(t, \boldsymbol{x}; \hat{c})$ the solution of (1.1) when the medium perturbations are $\delta\hat{c}^{-2}$ and the source term is (4.1). Denote by $\boldsymbol{d}[\hat{c}]$ the corresponding computed data:

$$d[\hat{c}](t, \boldsymbol{x}_r) = u(t, \boldsymbol{x}_r; \hat{c}) = \big(\mathcal{F}\delta\hat{c}^{-2}\big)(t, \boldsymbol{x}_r)\,.$$

We can implement an iterative imaging scheme based on calculating and minimizing the least-square functional

$$\tilde{\mathcal{J}}[\hat{c}] = \sum_{r=1}^{N_r}\int_{-\frac{T}{2}}^{\frac{T}{2}} \big|d(t, \boldsymbol{x}_r) - d[\hat{c}](t, \boldsymbol{x}_r)\big|^2\mathrm{d}t\,.$$

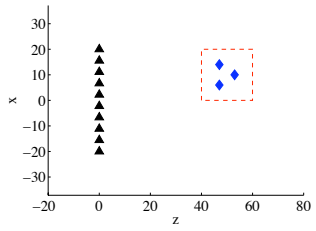

FIGURE 1. Numerical set-up: the triangles are the sensors of the array, the diamonds are the reflectors, the dashed lines determine the search window for the imaging functionals.

We then find in the Born approximation and when T is large enough (i.e. larger than the typical travel time and the typical time delay) that

$$\begin{aligned}\tilde{\mathcal{J}}[\hat{c}] &= \sum_{r=1}^{N_r} \int_{-\frac{T}{2}}^{\frac{T}{2}} \left|\left(\mathcal{F}\delta c^{-2}\right)(t,\boldsymbol{x}_r) - \left(\mathcal{F}\delta \hat{c}^{-2}\right)(t,\boldsymbol{x}_r)\right|^2 \mathrm{d}t \\ &= \iint_{\Omega^2} \mathcal{F}^*\mathcal{F}(\boldsymbol{x},\boldsymbol{x}')(\delta c^{-2}(\boldsymbol{x}) - \delta\hat{c}^{-2}(\boldsymbol{x}))(\delta c^{-2}(\boldsymbol{x}') - \delta\hat{c}^{-2}(\boldsymbol{x}'))\mathrm{d}\boldsymbol{x}\mathrm{d}\boldsymbol{x}' \\ &\approx \iint_{\Omega^2} \langle \mathcal{F}^*\mathcal{F}(\boldsymbol{x},\boldsymbol{x}')\rangle \, (\delta c^{-2}(\boldsymbol{x}) - \delta\hat{c}^{-2}(\boldsymbol{x}))(\delta c^{-2}(\boldsymbol{x}') - \delta\hat{c}^{-2}(\boldsymbol{x}'))\mathrm{d}\boldsymbol{x}\mathrm{d}\boldsymbol{x}' \,, \end{aligned} \tag{5.7}$$

where we use the statistical stability property of the normal operator. Applying a descent algorithm on $\tilde{\mathcal{J}}[\hat{c}]$ over $\hat{c}$ is much less computationally intensive than with the full MSR strategy, since it requires solving only one forward problem at each step of the algorithm. The essential observation here is that the residual in (5.6) corresponds to the residual in (5.7). Therefore, we can expect that the velocity model estimation based on the simultaneous sources will give estimates that are comparable to those obtained with (physical) measurements and successive numerical calculations based on simultaneous sources only, when in the scaling regime introduced above. We remark that the same random forcing should be used in each iteration, that is, the random forcing associated with the actual measured MSR matrix. Note, moreover, that if in fact the whole MSR matrix was measured in the physical experiment one could from this synthesize a "synthetic" simultaneous source experiment by convolution with simulated stationary random sources or randomly delayed sources.

6. Numerical illustrations

The numerical simulations presented in this section compare the image obtained with migration of the full MSR matrix and the one obtained with migration of a unique set of data collected with blended (randomly time delayed) sources.

We consider a three-dimensional homogeneous background medium with velocity $c_0 = 1$. We compute the image in the plane (x, z) and use the homogeneous background Green's function (1.4) and the Born approximation for the three reflectors we want to image. The source and receiver arrays are coincident and the $N_s = 10$ sensors are located at $(0, -20+4j)$, $j = 1, \ldots, 10$ (Figure 1). The pulse signal is the second derivative of a Gaussian with Fourier transform $\hat{f}(\omega) = \omega^2 \exp(-\omega^2)$. We

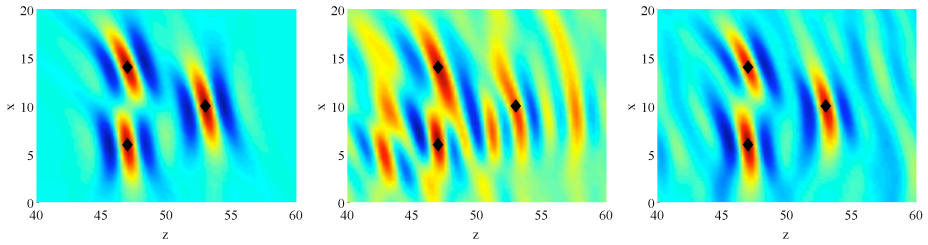

a) MSR **b)** BS $\tau_{\max} = 10$ **c)** BS $\tau_{\max} = 100$

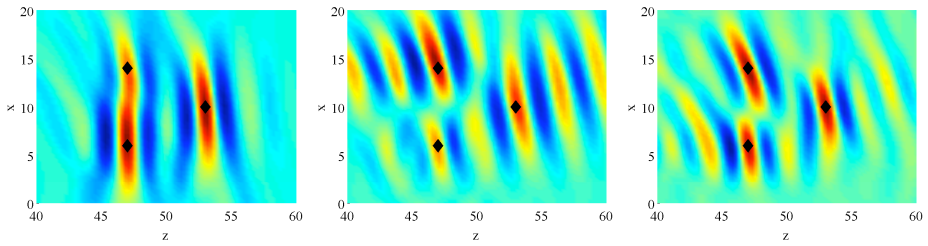

d) BS $\tau_{\max} = 0$ **e)** BS $\tau_{\max} = 10$ **f)** BS $\tau_{\max} = 100$

FIGURE 2. Images given by Kirchhoff migration of the full MSR matrix (a); migration of the data vector obtained with simultaneous sources without random time delays (d); migration of the data vector obtained with blended sources (BS) with random time delays uniformly distributed over $[-10, 10]$ for two realizations of the delays (b,e); migration of the data vector obtained with blended sources with random time delays uniformly distributed over $[-100, 100]$ for two realizations of the delays (c,f).

consider three point reflectors at locations $(47, 14)$, $(53, 10)$, $(47, 6)$ with the same reflectivity. The random time delays of the sources are independent and identically distributed random variables with uniform distribution over $[-\tau_{\max}, \tau_{\max}]$ and we test three different values for $\tau_{\max}$ and two different realizations in Figure 2. As expected by the theory, the image obtained with the data collected with blended sources is very similar to the one obtained with the full MSR matrix when $\tau_{\max}$ is large enough (here the time for a round trip from the array to the target is about 100). When $\tau_{\max}$ is small the image is unstable in that it depends on the particular realizations of the time delays.

7. Conclusion

We have presented a scheme for global imaging using incoherent simultaneous sources. A main focus of our analysis is the normal operator and we have been able to prove its statistical stability in our scaling regime. We have also discussed some important consequences for imaging and numerical forward simulations of our results. We have in fact been able to identify scaling regimes where we can obtain dramatically enhanced survey efficiency without sacrificing image quality.

The approach set forth here could indeed exploit and be combined with other blending approaches. For instance with enhanced signal processing and generation

capabilities one could use techniques developed in the area of wireless communications and seismic exploration to obtain enhanced simultaneity via partitioning of the frequency spectrum and specific source encoding.

Further work involves both extensions of the modeling and work on the imaging scheme. Regarding the modeling, results in the case of medium clutter and a general background function will be presented elsewhere. Regarding imaging schemes, further work focuses on analysis of optimal Kirchhoff migration and also a more general inverse scattering formulation incorporating ℓ_1 regularization.

We remark that we have not considered implementational aspects like parallelisation that will play a role in the trade-off of algorithms. We have rather presented a unified framework which shows how source blending in various implementations may play an important role in imaging.

Appendix A. Statistical stability for a continuum of point sources

When the point sources are close to each other (closer than a wavelength apart) than it is possible to model the process $n(t,\boldsymbol{x})$ as a zero-mean stationary (in time) Gaussian process with autocorrelation function

$$\langle n(t_1,\boldsymbol{y}_1)n(t_2,\boldsymbol{y}_2)\rangle = F(t_2-t_1)\delta(\boldsymbol{y}_2-\boldsymbol{y}_1)\theta\Big(\frac{\boldsymbol{y}_1+\boldsymbol{y}_2}{2}\Big)\,, \tag{A.1}$$

where the function θ describes the spatial support of the sources.

The product of second-order moments of the random process $n(t,\boldsymbol{x})$ is

$$\begin{aligned}&\langle n(t-s,\boldsymbol{y}_1)n(t-u,\boldsymbol{y}_2)\rangle\,\langle n(t'-s',\boldsymbol{y}_1')n(t'-u',\boldsymbol{y}_2')\rangle\\ &\quad = F(s-u)F(s'-u')\theta(\boldsymbol{y}_1)\delta(\boldsymbol{y}_1-\boldsymbol{y}_2)\theta(\boldsymbol{y}_1')\delta(\boldsymbol{y}_1'-\boldsymbol{y}_2')\,.\end{aligned}$$

The fourth-order moment of the Gaussian random process n is

$$\begin{aligned}&\langle n(t-s,\boldsymbol{y}_1)n(t-u,\boldsymbol{y}_2)n(t'-s',\boldsymbol{y}_1')n(t'-u',\boldsymbol{y}_2')\rangle\\ &\quad = F(s-u)F(s'-u')\theta(\boldsymbol{y}_1)\delta(\boldsymbol{y}_1-\boldsymbol{y}_2)\theta(\boldsymbol{y}_1')\delta(\boldsymbol{y}_1'-\boldsymbol{y}_2')\\ &\qquad +F(t'-t-s'+s)F(t'-t-u'+u)\theta(\boldsymbol{y}_1)\delta(\boldsymbol{y}_1-\boldsymbol{y}_1')\theta(\boldsymbol{y}_2)\delta(\boldsymbol{y}_2-\boldsymbol{y}_2')\\ &\qquad +F(t'-t-u'+s)F(t'-t-s'+u)\theta(\boldsymbol{y}_1)\delta(\boldsymbol{y}_1-\boldsymbol{y}_2')\theta(\boldsymbol{y}_2)\delta(\boldsymbol{y}_1'-\boldsymbol{y}_2)\,.\end{aligned}$$

Consequently, we have that for any $T>0$

$$\begin{aligned}&\int_{-\frac{T}{2}}^{\frac{T}{2}}\int_{-\frac{T}{2}}^{\frac{T}{2}}\Big(\langle n(t-s,\boldsymbol{y}_1)n(t-u,\boldsymbol{y}_2)n(t'-s',\boldsymbol{y}_1')n(t'-u',\boldsymbol{y}_2')\rangle\\ &\qquad\qquad -\langle n(t-s,\boldsymbol{y}_1)n(t-u,\boldsymbol{y}_2)\rangle\,\langle n(t'-s',\boldsymbol{y}_1')n(t'-u',\boldsymbol{y}_2')\rangle\Big)\mathrm{d}t\mathrm{d}t'\\ &\quad = S_T(s-s',u-u')\theta(\boldsymbol{y}_1)\delta(\boldsymbol{y}_1-\boldsymbol{y}_1')\theta(\boldsymbol{y}_2)\delta(\boldsymbol{y}_2-\boldsymbol{y}_2')\\ &\qquad +S_T(s-u',u-s')\theta(\boldsymbol{y}_1)\delta(\boldsymbol{y}_1-\boldsymbol{y}_2')\theta(\boldsymbol{y}_2)\delta(\boldsymbol{y}_1'-\boldsymbol{y}_2)\,,\end{aligned} \tag{A.2}$$

with S_T defined by (3.12). We then get the same formulas as in the discrete model.

Appendix B. Resolution analysis

We consider the kernel:

$$\mathcal{I}_\omega(\boldsymbol{x},\boldsymbol{x}') = \sum_{r=1}^{N_r}\overline{\hat{G}}\big(\omega,\boldsymbol{x}_r,\boldsymbol{x}\big)\hat{G}\big(\omega,\boldsymbol{x}_r,\boldsymbol{x}'\big)\,.$$

We assume that the points $(\boldsymbol{x}_r)_{r=1}^{N_r}$ are at the surface $\Sigma = \{\boldsymbol{y} \in \mathbb{R}^3, y_3 = 0\}$ and are close to each other (closer than half-a-wavelength) so that a continuum approximation can be used:

$$\mathcal{I}_\omega(\boldsymbol{x}, \boldsymbol{x}') = \int_\Sigma \rho(\boldsymbol{x}_r)\overline{\hat{G}}\big(\omega, \boldsymbol{x}_r, \boldsymbol{x}\big)\hat{G}\big(\omega, \boldsymbol{x}_r, \boldsymbol{x}'\big)\mathrm{d}\sigma(\boldsymbol{x}_r)\,,$$

where ρ is the surface density of receivers. In the high-frequency asymptotics, for $\boldsymbol{x} = \boldsymbol{x}'$, we have

$$\mathcal{I}_\omega(\boldsymbol{x}, \boldsymbol{x}) = \int_\Sigma \rho(\boldsymbol{x}_r)\mathcal{A}(\boldsymbol{x}, \boldsymbol{x}_r)^2\mathrm{d}\sigma(\boldsymbol{x}_r)\,.$$

For $|\boldsymbol{x} - \boldsymbol{x}'|$ of the order of the wavelength, we find

$$\mathcal{I}_\omega(\boldsymbol{x}, \boldsymbol{x}') \simeq \int_\Sigma \rho(\boldsymbol{x}_r)\mathcal{A}(\boldsymbol{x}', \boldsymbol{x}_r)^2 \exp\big(-i\omega\nabla_{\boldsymbol{x}'}\mathcal{T}(\boldsymbol{x}', \boldsymbol{x}_r)\cdot(\boldsymbol{x} - \boldsymbol{x}')\big)\mathrm{d}\sigma(\boldsymbol{x}_r)\,.$$

If, additionally, we assume that the background is homogeneous $c(\boldsymbol{x}) = c_0$, then $\mathcal{T}(\boldsymbol{x}', \boldsymbol{x}_r) = |\boldsymbol{x}' - \boldsymbol{x}_r|/c_0$ and $\mathcal{A}(\boldsymbol{x}', \boldsymbol{x}_r) = 1/(4\pi|\boldsymbol{x}' - \boldsymbol{x}_r|)$ and we have

$$\mathcal{I}_\omega(\boldsymbol{x}, \boldsymbol{x}') \simeq \frac{1}{(4\pi)^2}\int_\Sigma \rho(\boldsymbol{x}_r)\frac{1}{|\boldsymbol{x}' - \boldsymbol{x}_r|^2}\exp\Big(i\frac{\omega}{c_0}\frac{\boldsymbol{x}_r - \boldsymbol{x}'}{|\boldsymbol{x}_r - \boldsymbol{x}'|}\cdot(\boldsymbol{x} - \boldsymbol{x}')\Big)\mathrm{d}\sigma(\boldsymbol{x}_r)\,.$$

This expression gives the width and the form of the function $\mathcal{I}_\omega(\boldsymbol{x}, \boldsymbol{x}')$ along the diagonal band $\boldsymbol{x} \simeq \boldsymbol{x}'$. If the diameter a of the array (i.e. the support of ρ) is smaller than the distance from the array to $\boldsymbol{x}'$, then then we find the standard Rayleigh resolution formulas. If the diameter of the array is of the same order as or larger than the distance from the array to $\boldsymbol{x}'$, then we find that the resolution is of the order of the wavelength.

Using stationary phase arguments, we obtain for $|\boldsymbol{x} - \boldsymbol{x}'|$ much larger than the typical wavelength:

$$\mathcal{I}_\omega(\boldsymbol{x}, \boldsymbol{x}') \simeq \frac{\rho(\boldsymbol{x}_0)}{(4\pi)^2}\frac{2\pi c_0(x_3 - x_3')^2}{|\boldsymbol{x} - \boldsymbol{x}'|^3}\frac{i}{\omega}\mathrm{sgn}(x_3 - x_3')\exp\Big(-i\frac{\omega}{c_0}|\boldsymbol{x} - \boldsymbol{x}'|\Big)\,,$$

where $\boldsymbol{x}_0$ is the intersection of the ray going through $\boldsymbol{x}$ and $\boldsymbol{x}'$ with the surface $y_3 = 0$:

$$\boldsymbol{x}_0 = \frac{x_3\boldsymbol{x}' - x_3'\boldsymbol{x}}{x_3 - x_3'}\,.$$

This expression gives the long-distance decay of the function $\mathcal{I}_\omega(\boldsymbol{x}, \boldsymbol{x}')$ for $\omega|\boldsymbol{x} - \boldsymbol{x}'|/c_0 \gg 1$.

References

1. H. Ammari, E. Bretin, J. Garnier, and A. Wahab, *Noise source localization in an attenuating medium*, SIAM J. Appl. Math., 72 (2012), pp. 317-336.
2. C. Bagaini, *Acquisition and processing of simultaneous vibroseis data*, Geophysical Prospecting, 58 (2010), pp. 81-99.
3. A.J. Berkhout, *Changing the mindset in seismic data acquisition*, The Leading Edge, 27 (2009), pp. 924-938.
4. A.J. Berkhout, G. Blacquiere, and D.J. Verschuur, *The concept of double blending: Combining incoherent shooting with incoherent sensing*, Geophysics, 74 (2009), pp. A59-A62.
5. N. Bleistein, J.K. Cohen, and J.W. Stockwell Jr, *Mathematics of multidimensional seismic imaging, migration, and inversion*, Springer Verlag, New York, 2001.
6. W. Dai and J. Schuster, *Least-squares migration of simultaneous sources data with a deblurring filter*, SEG Houston 2009 International exposition and Annual Meeting.
7. M. de Hoop and K. Sølna, *Estimating a Green's function from field-field correlations in a random medium*, SIAM J. Appl. Math., 69 (2009), pp. 909-932.

8. M. Fink, D. Cassereau, A. Derode, C. Prada, P. Roux, M. Tanter, J.-L. Thomas, and F. Wu, *Time-reversed acoustics*, Reports on Progress in Physics, 63 (2000), pp. 1933-1995.
9. J.-P. Fouque, J. Garnier, G. Papanicolaou, and K. Sølna, *Wave propagation and time reversal in randomly layered media*, Springer, New York, 2007.
10. J. Garnier and G. Papanicolaou, *Passive sensor imaging using cross correlations of noisy signals in a scattering medium*, SIAM J. Imaging Sciences, 2 (2009), pp. 396-437.
11. J. Garnier and G. Papanicolaou, *Resolution analysis for imaging with noise*, Inverse Problems, 26 (2010), 074001.
12. J. Garnier and G. Papanicolaou, *Fluctuation theory of ambient noise imaging*, CRAS Geoscience 343 (2011), pp. 502-511.
13. J. Garnier and K. Sølna, *Filtered Kirchhoff migration of cross correlations of ambient noise signals*, Inverse Problems and Imaging, 5 (2011), pp. 371-390.
14. G. Hampson, J. Stefani, and F. Herkenhoff, *Acquisition using simultaneous sources*, The Leading Edge, 27 (2008), pp. 918-923.
15. H. Yao, R. D. van der Hilst, and M. V. de Hoop, *Surface-wave array tomography in SE Tibet from ambient seismic noise and two-station analysis I. Phase velocity maps*, Geophysical Journal International, 166 (2006), pp. 732-744.

Center for Computational and Applied Mathemematics, Purdue University, West Lafayette, IN 47907
E-mail address: mdehoop@purdue.edu

Laboratoire de Probabilités et Modèles Aléatoires, Université Paris VII, Site Chevaleret, 75205 Paris Cedex 13, France
E-mail address: fedrizzi@math.univ-paris-diderot.fr

Laboratoire de Probabilités et Modèles Aléatoires & Laboratoire Jacques-Louis Lions, Université Paris VII, Site Chevaleret, 75205 Paris Cedex 13, France
E-mail address: garnier@math.jussieu.fr

Department of Mathematics, University at California at Irvine, Irvine, CA 92697
E-mail address: ksolna@math.uci.edu